

## 1. MOTIVATION

### Field of Interest: UXO Detection

- Problem: hazard potential due to buried unexploded ordnance
- Aim: reliable detection of target objects by an improved interpretation of geomagnetic survey data

### Experimental Design:

- Simulation of the anomaly field for realistic survey conditions
- Implementation of an adequate artificial neural network
- Building a model to recognize the magnetic signature of potential target objects



Fig. 1: Cluster munition (AzVision, 2020)

## 3. PREPROCESSING OF THE INPUT DATA

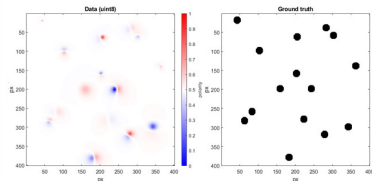


Fig. 3: Processing results: Normalized uint8 RGB image (left). Labeled mask (right)

## 2. GENERATION OF REPRESENTATIVE SURVEY DATA

### Data basis:

$$B(P) = \frac{\mu_0 m}{4\pi r^3} [3(\hat{m} \cdot \hat{r})\hat{r} - \hat{m}]$$

### Experimental Field

Location	Freiberg = 49400 nT
Investigation Area	200 x 200 m
Measuring & Profile Distance	$\Delta x = 0.5$ m $\Delta y = 0.5$ m
Gaussian Noise	none / 0,1 / 0,3 nT
<b>Object Properties</b>	
Number per Field	1 to 20
Depth	0 to 15 m
Sphere Radius	0,01 to 0,1 m
Dipole Axis Orientation	Random

Tab. 1: General simulation parameter

- Calculating the magnetic dipole potential  $B(P)$  of a homogeneously magnetized sphere by Blakely (1996), where  $P$  denotes the observation point
- Considering the geographical latitude
- Simulation routine by Gödickmeier (2020)

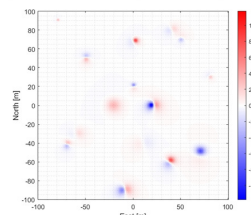
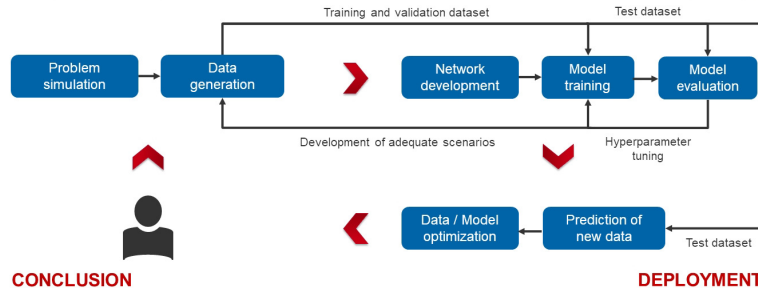


Fig. 2: Simulated unnoised multi-dipole scenario

### Compression:

- Raw: Fig. 2
  - [400x400] real-value double matrix
  - Compressed: Fig. 3 left
  - [400x400x3] normalized uint8 RGB matrix
- ### Labeling:
- Mask sample containing labels for each anomaly to be detected; Fig. 3 right
  - Center corresponds to exact dipole position
  - Radius indicates detection accuracy

## DATA PREPARATION



## CONCLUSION

## 9. DISCUSSION ON PREVIOUS STUDIES

### Data-related optimization approaches:

- Asinh not applied further because of generating artifacts in the presence of noise
- Colomap with 3 channels applied further because of accelerating the learning process during early epochs

### Model-related optimization approaches:

- Tuning of batch size and dropout deliver no significant improvement to training as well as prediction
- Reduced steps per epoch causes a great gain in time for training with qualitatively still accurate predictions

Learning Rate (Opt. „Adam“)	0.001
Epochs	30
Batch Size	32 Samples
Steps per Epoch	250
RGB Channels (Colomap)	[1 1 1]

Tab. 3: General training information and hyperparameter

## 4. NETWORK ARCHITECTURE

### U-Net:

- Convolutional neural network to perform semantic image segmentation
- Input: 30000 samples in total (70 % Training set; 30 % Evaluation set)
- a) Contracting path → Feature extraction
- b) Bottleneck → Passes tensor dimension
- c) Expansive path → Localization of features
- Output: Segmentation map (Pixel-wise prediction for the input image)

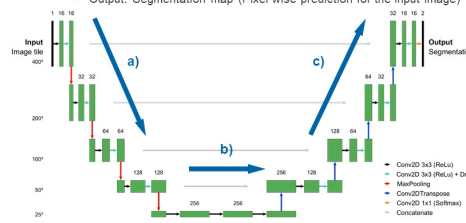


Fig. 4: U-Net architecture for semantic image segmentation (based on Ronneberger et al. 2015)

## 5. TRAINING

### Model History:

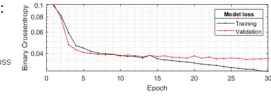


Fig. 5: Exemplary loss curve for a model based on Tab. 2

Learning Rate (Opt. „Adam“)	0.001
Epochs	30
Batch Size	32 Samples
Steps per Epoch	525
RGB Channels (Colomap)	[1 1 1]

Tab. 2: General training information and hyperparameter

### Binary Crossentropy Loss:

$$L = -\frac{1}{N} \sum_{i=1}^N y_i^{\text{true}} \log(f(x_i^{\text{predicted}}; W)) + (1 - y_i^{\text{true}}) \log(1 - f(x_i^{\text{predicted}}; W))$$

$x$  – Ground truth;  $y$  – Prediction;  $W$  – Weights

- Training and evaluation is performed using the Keras API for Tensorflow

## 6. EVALUATION

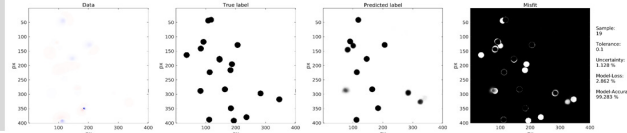


Fig. 6: Predicted sample with 19 randomly generated anomalies; Input: Data & ground truth (left). Output: Segmentation map & calculated misfit (right)

### Criteria:

- Progression of cross validation loss during training process (Fig. 5 upper panel)
  - Fast training dynamic; overfitting: Drifting apart of training and validation curve
- RMS error from the deviation between ground truth and prediction (Fig. 7)
  - Generally low loss; great performance; more right-skewed distribution preferred
- Misfit plot of ground truth and prediction for visual evaluation of individual samples
  - Extremely weak signals due to depth/size-ratio not detectable
  - Sufficiently strong signals detected with high certainty and high position accuracy

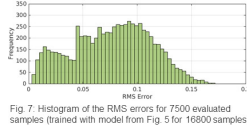


Fig. 7: Histogram of the RMS errors for 7500 evaluated samples (trained with model from Fig. 5 for 16500 samples)

## 11. OUTLOOK

### Opportunities for further improvement:

- Increase the complexity of the data basis
  - Additive, irregular background field representing an individual regional field (e.g. Fig. 9)
  - Additional non-target structures (e.g. archaeological structures, cables, pipelines, etc.)
- Adjustment of ground truth parameters
  - Gray-scale labels carrying depth information
  - Label radii determining achievable position accuracy

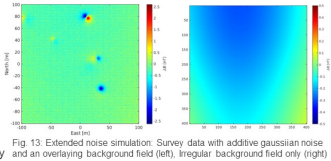


Fig. 13: Extended noise simulation: Survey data with additive gaussian noise and an overlaying background field (left). Irregular background field only (right)

## 10. PRELIMINARY MODEL RESULT

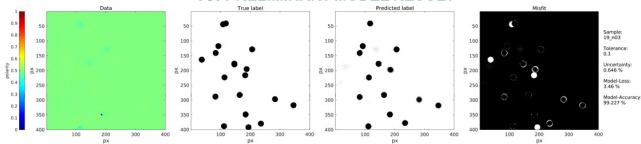


Fig. 11: Predicted sample with 19 randomly generated anomalies; Input: Data & ground truth (left). Output: Segmentation map & calculated misfit (right)

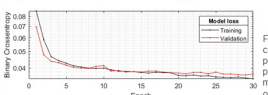


Fig. 12: Loss curve for the preliminary model based on Tab. 3

- Low loss and great generalization (Fig. 12) achieved by including various noise levels and adequate amount of input data
- High accuracy in localizing individual anomalies by transition to 3 RGB channels and reduction of artifacts
- Few weak signals undetectable due to superposition, noise or technical limitation while measuring

## 8. MODEL-RELATED OPTIMIZATION APPROACHES

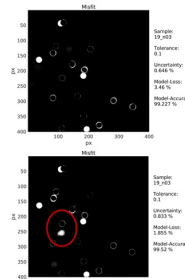


Fig. 10: Misfit: Original data (top), Arasine hyperbolicus (down), 3-Channel-Colomap

- ### Steps per Epoch
- Reduction from 525 to 250 batches; compare with Fig. 9 lowest panel
  - Time saving with similar results
  - Asinh creates artifacts due to noise

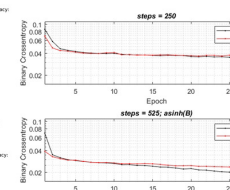


Fig. 9: Loss curves for reduced number of steps per epoch in combination with Arasine hyperbolicus, 3-Channel-Colomap

## 7. DATA-RELATED OPTIMIZATION APPROACHES

### 3-Channel-Colomap:

- Accelerates training dynamics
- Faster adjustment of weights in the first epochs → steeper gradient
- More information processed at the same time

### Arasine hyperbolicus:

- Scales signals for an improved recognition
- Lower losses than unscaled scenario after 30 epochs
- Intensifies overfitting (uncertainties due to noisy samples)
- Manipulates signal-to-noise ratio (inflated noise)

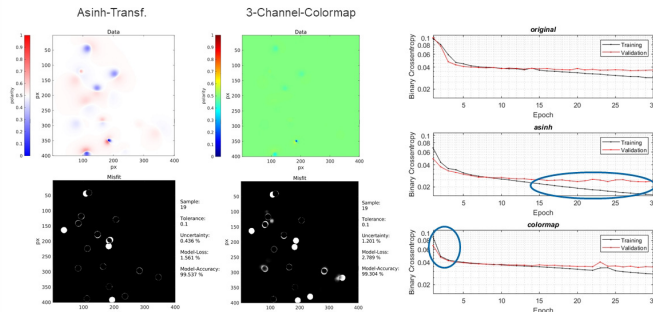


Fig. 8: Transformed data and Misfit (belonging to Fig. 6): Arasine hyperbolicus (left), 3-Channel-Colomap all three RGB-channels (right)



Fig. 9: Loss curves of training with transformed data in comparison to original input data

## REFERENCES

[1] AzVision (2020). <https://de.azvision.com/news/91526-armenien-setzte-streumung-bei-mehreren-angriffen-auf-aserbadshan-ein.html> (retrieved on November 21, 2021)

[2] Blakely, R. J. (1996). Potential theory in gravity and magnetic applications. Cambridge: Univ. Press. isbn: 0-521-57547-8.

[3] Gödickmeier, P. (2020). Methodische Untersuchungen zur Entwicklung einer hochauflösenden Magnetsensoreinheit für Drohnen. Masterthesis, Institute for Geophysics and Geoinformatics, TU Bergakademie Freiberg.

[4] Olaf Ronneberger, Philipp Fischer, and Thomas Brox. (2015). U-net: convolutional networks for biomedical image segmentation. arXiv: 1505.04597.

## ACKNOWLEDGEMENT

Supported by the Deutsche Forschungsgemeinschaft (DFG) – 397252409

M. Sc. Peggy Gödickmeier

Gustav-Zeuner-Str. 12 | 09599 Freiberg | [peggy.goeckmeier@geophysics.tu-freiberg.de](mailto:peggy.goeckmeier@geophysics.tu-freiberg.de) | DGG 07.03.2022